

# Boltzmann transport and residual conductivity in bilayer graphene

Shaffique Adam and S. Das Sarma

*Condensed Matter Theory Center, Department of Physics,  
University of Maryland, College Park, MD 20742-4111, USA*

(Dated: March 21, 2008)

A Drude-Boltzmann theory is used to calculate the transport properties of bilayer graphene. We find that for typical carrier densities accessible in graphene experiments, the dominant scattering mechanism is overscreened Coulomb impurities that behave like short-range scatterers. We anticipate that the conductivity  $\sigma(n)$  is linear in  $n$  at high density and has a plateau at low density corresponding to a residual density of  $n^* = \sqrt{n_{\text{imp}} \tilde{n}}$ , where  $\tilde{n}$  is a constant which we estimate using a self-consistent Thomas-Fermi screening approximation to be  $\tilde{n} \approx 0.01$   $q_{\text{TF}}^2 \approx 140 \times 10^{10} \text{ cm}^{-2}$ . Analytic results are derived for the conductivity as a function of the charged impurity density. We also comment on the temperature dependence of the bilayer conductivity.

PACS numbers: 81.05.Uw; 72.10.-d, 73.40.-c

## I. INTRODUCTION

The recent experimental realization of a single layer of carbon atoms arranged in a honeycomb lattice has prompted much excitement in both the theoretical and experimental physics communities (For a recent review, see Ref. 1 and references therein). The focus of the current work is on bilayer graphene which has received less attention both theoretically and experimentally, but is nonetheless of equal importance both for technological application and for fundamental science. Bilayer graphene is two monoatomic layers of graphene separated by about 0.3 nm, which is the interplane distance in bulk graphite. Similar to single layer graphene, bilayer graphene has been realized experimentally through the mechanical exfoliation of graphite onto  $\text{SiO}_2$  substrates.<sup>1</sup> While the band structure of a single layer of graphene has a linear dispersion, theoretically bilayer graphene has a quadratic dispersion with an effective mass of about  $0.03 m_e$  making it similar to the regular two dimensional electron gas (2DEG). Despite the quadratic spectrum, bilayer graphene shares two important features with single layer graphene (hereafter referred to simply as graphene) that distinguish it from regular 2DEGs. First, the bilayer effective Hamiltonian<sup>2,3,4,5,6</sup> is chiral which gives rise to the anomalous integer quantum hall effect.<sup>7</sup> Second, unbiased bilayer graphene is a semimetal implying that one continuously moves from electron-like carriers for positive gate voltages to hole-like carriers for negative gate voltages without any gap in the spectrum. We note that although recent experiments<sup>8</sup> on graphene bilayers have been able to open a gap by connecting the upper layer to an external top gate, here we ignore this additional degree of freedom.<sup>9,10</sup>

By considering the gapless bilayer situation, the low density transport resembles that of single layer where Coulomb impurities in the substrate create an inhomogeneous density profile breaking the system into puddles of electrons and holes. The bulk residual density  $n^*$  induced by these impurities has been calculated for single layer graphene<sup>11,12</sup> which shows agreement with recent

experimental studies.<sup>13,14,15</sup> The high density transport in single layer graphene with screened Coulomb impurities was discussed in Refs. 11,16,17,18,19,20. The goal of the present work is to generalize these high-density and low-density single-layer graphene Boltzmann transport theories to the case of graphene bilayers. We note that the Boltzmann transport theory developed here ignores the effects of phase-coherence which was studied in Refs. 21,22.

## II. BILAYER HAMILTONIAN AND BOLTZMANN TRANSPORT

The effective Hamiltonian for bilayer graphene is now well established in the theoretical literature (See Refs. 2, 3,4,5,6,23,24,25). First principles and band structure calculations show that at both very small energies and very large energies, bilayer graphene has a linear spectrum. For energies  $2 \times 10^{-3} \text{ eV} \lesssim \epsilon \lesssim 0.1 \text{ eV}$  bilayer graphene has a quadratic spectrum (see e.g. Refs. 2,4). In principle, bilayer graphene should have a complicated crossover Hamiltonian moving from linear to quadratic and back to linear as one increased the carrier density. To our knowledge, a theoretical framework to understand the structure and effects of chirality within this crossover has not yet been developed. However, as we argue below, charged impurities in the substrate induce a residual density  $n^*$  in bilayer graphene that corresponds to a typical Fermi energy  $\epsilon \gtrsim 0.01 \text{ eV}$  which is larger than the lower energy scale for using the quadratic Hamiltonian, and the range of experimental gate voltages  $V_g \lesssim 50 \text{ V}$  induces a maximum carrier density with Fermi energy  $\epsilon \lesssim 0.1 \text{ eV}$  which is comparable to the limit where the low-energy effective quadratic Hamiltonian begins to break down. Therefore, for realistic samples, the condition  $2 \times 10^{-3} \text{ eV} \lesssim \epsilon \lesssim 0.1 \text{ eV}$  is mostly satisfied and the quadratic Hamiltonian  $\mathcal{H}$  proposed by McCann and Falko should be an excellent approximation, where in addition bilayer graphene is weakly interacting in this energy window. In what follows, we use<sup>2</sup>

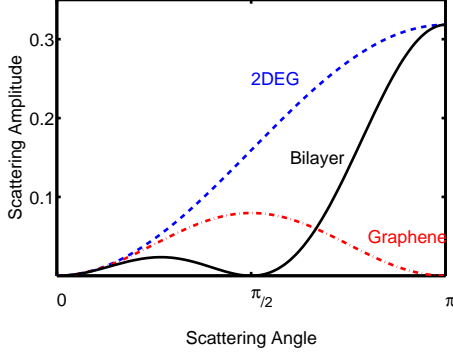


FIG. 1: (Color online) Scattering cross-section as a function of angle. Unlike single layer graphene, both bilayer graphene and 2DEG are dominated by backscattering.

$$\mathcal{H} = -\frac{1}{2m} \begin{pmatrix} 0 & [p_x - ip_y]^2 \\ [p_x + ip_y]^2 & 0 \end{pmatrix}. \quad (1)$$

This Hamiltonian can be diagonalized giving  $\epsilon_k = \pm \hbar^2 k^2 / 2m$  where  $m = 2\gamma_1 \hbar^2 / (3\gamma_0^2 a^2) \approx 0.033 m_e$ , and  $\gamma_0 \approx 3.16$  eV is the in-plane coupling and  $\gamma_1 \approx 0.39$  eV is the out of plane coupling,  $a \approx 0.246$  nm is the lattice constant and  $m_e$  is the electron mass. The eigenvectors  $\xi_{\pm} = (e^{-i2\theta_k}, \pm 1)$  give the aforementioned chiral properties where  $\mathbf{k} = k \exp(i\theta_k)$ .

Using this diagonal basis, one can calculate the scattering time  $\tau$  using the Boltzmann transport theory<sup>26</sup> to find

$$\frac{\hbar}{\tau(\epsilon_k)} = 2\pi \sum_{k'} n_{\text{imp}} |\tilde{v}(q)|^2 (1 - \hat{\mathbf{k}} \cdot \hat{\mathbf{k}}') F_{\mathbf{k}\mathbf{k}'} \delta(\epsilon_k - \epsilon_{k'}), \quad (2)$$

where the momentum transfer  $q = |\mathbf{k} - \mathbf{k}'| = 2k_F \sin(\theta/2)$ ,  $\tilde{v}(x)$  is the screened scattering impurity potential and  $\hat{\mathbf{k}} \cdot \hat{\mathbf{k}}' = \cos\theta$ . The effects of chirality are captured in  $F_{\mathbf{k}\mathbf{k}'}$ . For a regular 2DEG whose Hamiltonian is not chiral, we have  $F(\theta) = 1$ , whereas  $F(\theta) = (1 + \cos\theta)/2$  for graphene and  $F(\theta) = (1 + \cos 2\theta)/2$  for bilayer graphene. The term  $(1 - \hat{\mathbf{k}} \cdot \hat{\mathbf{k}}') F_{\mathbf{k}\mathbf{k}'}$  determines the scattering cross-section which has been plotted in Fig. 2. We observe that in contrast to single layer graphene, both bilayer graphene and the 2DEG are dominated by backscattering ( $\theta = \pi$ ). Introducing  $x = q/(2k_F)$ , we find

$$\frac{\hbar}{\tau} = \begin{cases} n_{\text{imp}} \frac{16m}{\pi} \int_0^1 dx |\tilde{v}(x)|^2 \frac{(x-2x^3)^2}{\sqrt{1-x^2}} & \text{for bilayers,} \\ n_{\text{imp}} \frac{4\epsilon_F}{\pi v_F^2} \int_0^1 dx |\tilde{v}(x)|^2 x^2 \sqrt{1-x^2} & \text{for graphene,} \end{cases} \quad (3)$$

where the single layer graphene result was reported previously in Refs. 11,19,27.

TABLE I: Summary of Boltzmann transport results in 2d electron gas (2DEG), single layer graphene and bilayer graphene. For screened Coulomb scattering results in 2DEG and bilayer graphene we assume that  $q_{\text{TF}}/2k_F > 1$  (see text), and observe that arising from different physics, screened Coulomb scattering gives  $\sigma \sim n$  in all three cases.

	2DEG	Graphene	Bilayer
Bare Coulomb Scattering	$\sigma \sim n^2$	$\sigma \sim n$	$\sigma \sim n^2$
Screened Coulomb	$\sigma \sim n$	$\sigma \sim n$	$\sigma \sim n$
Short-range Scattering	$\sigma \sim n$	$\sigma \sim \text{const}$	$\sigma \sim n$

Before calculating the Boltzmann conductivity  $\sigma = (2e^2/h)k_F v_F \tau$ , we first use dimensional arguments to determine the dependence of conductivity on carrier density. In 2DEGs and bilayer graphene the Fermi velocity  $v_F = \hbar k_F / m$  depends on carrier density through  $n \sim k_F^2$  while the inverse screening length  $q_{\text{TF}} = 4\pi e^2 / (\kappa \hbar^2)$  is density independent. Since the gas density parameter  $r_s \sim v_F^{-1}$ , it scales as  $n^{-1/2}$ . This is all in sharp contrast to single layer graphene where  $v_F \approx 10^6$  m/s is constant and  $q_{\text{TF}} = 4\kappa_F r_s$  depends on carrier density, and  $r_s = e^2 / (\kappa v_F) \approx 0.8$  is a density independent constant that depends mostly on the dielectric constant of the substrate.

One finds that for bilayer graphene  $\sigma \sim k_F^2 \tau$ , and that for unscreened Coulomb impurities  $\tau_C \sim k_F^2$  giving  $\sigma_C \sim n^2$ , whereas overscreened Coulomb scatterers behave similar to white-noise disorder giving density independent  $\tau$  and  $\sigma \sim n/n_{\text{imp}}$  (this is similar to a low-density 2DEG, where Coulomb scatterers are strongly screened if  $q_{\text{TF}} \gg 2k_F$ ). Writing  $\sigma(n) \sim n^\alpha$ , we note that  $\alpha = 1$  in both the linear and quadratic Hamiltonians arising from very different reasons (See Table I). The solution within a crossover between a quadratic and linear Hamiltonian (see above) is beyond the scope of this work, but we observe that approaching the crossover from either side gives  $\alpha \geq 1$ , and for Coulomb scatterers located at the SiO<sub>2</sub> interface, we have  $\alpha \leq 2$ . In what follows we focus on the experimentally relevant regime, where we assume that  $q_{\text{TF}}/2k_F > 1$  which is typically called the low density regime in 2DEG literature.<sup>28</sup> In this context, even in GaAs heterostructures (where  $m \approx 0.07 m_e$ ) moving to higher density results in a complicated crossover where the exponent  $\alpha$  slowly decreases with increasing density as other scattering mechanisms come into play.<sup>28</sup>

In single layer graphene, it was shown by Refs. 29,30 that for  $q \leq 2k_F$  the static dielectric function calculated in the Random Phase Approximation is identical

to that of the much simpler Thomas-Fermi approximation. A similar result holds for 2DEGs. While it is not clear if this holds in bilayer where the polarizability has only been calculated numerically (See Ref. 31), these results indicate that Thomas-Fermi approximation (which allows for analytical results) should capture both qualitatively and quantitatively the transport properties of bilayer graphene. Within the Thomas-Fermi approximation, the potential of a charged impurity located at a distance  $d$  from the substrate is

$$\tilde{v}(q) = \frac{2\pi e^2}{\kappa} \frac{e^{-qd}}{q + q_{\text{TF}}} \approx \frac{\pi \hbar^2}{2m}, \quad (4)$$

where in the second equation we have used the further approximation (also called “complete screening approximation”) that  $q_{\text{TF}} = 4me^2/(\kappa \hbar^2) \sim 1 \text{ nm}^{-1}$  is larger than the maximum transferred momentum  $q \lesssim 0.3 \text{ nm}^{-1}$ . Herein lies an important difference between single layer graphene and bilayer graphene. For single layer graphene  $q_{\text{TF}} = 4k_{\text{F}}/s$  depends on density, so that both the screened and unscreened Coulomb potential scale as  $k_{\text{F}}^{-1}$ . It is this property of single layer graphene that gives rise to the conductivity with Coulomb scatterers being linear in density and the inapplicability of Gaussian white-noise models (i.e. zero-range scattering) to capture the transport properties. In contrast, for bilayer graphene and 2DEG,  $q_{\text{TF}}$  is a density independent constant which is larger than the typical momentum transferred in current experiments, and therefore the strong screening approximation ( $q_{\text{TF}} > 2k_{\text{F}}$ ) applies except at very high carrier densities. In this context, bilayer graphene is much more similar to 2D Si MOSFETs than to single layer graphene. Analytic results for the conductivity can be obtained both in the limit  $d \rightarrow 0$  and  $2k_{\text{F}}/q_{\text{TF}} \rightarrow 0$ . Keeping both to leading order, we find

$$\sigma(n) \approx \frac{4e^2}{\pi \hbar} \frac{n}{n_{\text{imp}}} \left[ 1 + \frac{1216}{105\sqrt{\pi}} \sqrt{n}(d + q_{\text{TF}}^{-1}) \right]. \quad (5)$$

The result  $\sigma = (4e^2/\pi \hbar)(n/n_{\text{imp}})$ , where conductivity is linear in density is valid for  $d^{-1}, q_{\text{TF}} \gg 2k_{\text{F}}$ , although we expect deviations from this linear behavior for  $n \geq 6 \times 10^{11} \text{ cm}^{-2}$ , a regime, which in principle should be accessible in future experiments. We note that the linear in density behavior was anticipated in Ref. 5 and in Ref. 24, but we point out that the low density saturation in Ref. 5 arises from a completely different and universal mechanism<sup>23,25</sup> that we believe is unobservable in current bilayer graphene samples because of the large and non-universal  $n^*$  arising from the disorder induced electron-hole puddles.<sup>11,32</sup> In the following section we calculate the voltage fluctuations and residual density induced by charged impurities.

### III. LOW DENSITY RESIDUAL DENSITY

This section follows closely the derivation in Refs. 11,33 and applying the same formalism to the case of bilayer

graphene. We consider  $N_{\text{imp}}$  impurities located at the points  $\{r_i\}$  in a 2D plane. If each impurity has a potential  $\phi(r)$ , then the disorder averaged potential

$$\begin{aligned} \bar{V} &= \int d\mathbf{r}_1 d\mathbf{r}_2 \cdots P[\mathbf{r}_1] P[\mathbf{r}_2] \cdots \sum_{i=1}^{N_{\text{imp}}} \phi(r_i), \\ &= n_{\text{imp}} \tilde{\phi}(q=0), \end{aligned} \quad (6)$$

where to get the second line we have assumed that the impurities are uncorrelated and uniformly distributed. For sample area  $A$ ,  $n_{\text{imp}} = N_{\text{imp}}/A$ ,  $P[\mathbf{r}_i] = A^{-1}$  and  $\tilde{\phi}(q)$  is the 2D Fourier Transform of the impurity potential  $\phi(r)$ . For example, the real space Coulomb potential for an impurity located a distance  $d$  from the graphene (or bilayer) plane,  $\phi(r) = (e^2/\kappa)[\mathbf{r}^2 + d^2]^{-1/2}$ . This gives for the bare potential  $\tilde{\phi}_0(q) = (2\pi e^2/\kappa) \exp(-qd)/q$ . Using the Thomas-Fermi dielectric function  $\epsilon(q) = 1 + q_{\text{TF}}/q$  gives the screened Thomas-Fermi potential shown in Eq. 4. Since the static polarizability at  $q \rightarrow 0$  is related to the density of states  $\nu$  by the compressibility sum rule, the result for the disorder averaged potential  $\bar{V} = n_{\text{imp}}/\nu$  is actually quite general. For bilayer graphene  $\nu$  is constant, and the threshold voltage shift can be immediately obtained from  $\bar{n} = \bar{V}\nu = n_{\text{imp}}$ . It is the property that  $q_{\text{TF}}$  is independent of carrier density that explains why the threshold voltage shift in bilayers is  $\bar{n} = n_{\text{imp}}$ , which is in contrast to graphene<sup>11</sup> where the density dependent inverse screening length gives  $\bar{n} = n_{\text{imp}}^2/4n^*$ . This non-linear dependence of the threshold voltage on charged impurity density in monolayer graphene has recently been verified experimentally.<sup>14</sup>

The disorder averaged potential fluctuations  $\langle V^2 \rangle$  are obtained in a similar fashion.

$$\begin{aligned} \langle V^2 \rangle &= \int d\mathbf{r}_1 d\mathbf{r}_2 \cdots P[\mathbf{r}_1] P[\mathbf{r}_2] \cdots \sum_{i,j=1}^{N_{\text{imp}}} \phi(r_i) \phi(r_j), \\ \langle V^2 \rangle - \bar{V}^2 &= \int d\mathbf{r}_1 d\mathbf{r}_2 \cdots P[\mathbf{r}_1] P[\mathbf{r}_2] \cdots \sum_{i,j=1}^{N_{\text{imp}}} \phi(r_i) \phi(r_j), \\ &= n_{\text{imp}} \int \frac{d\mathbf{q}}{(2\pi)^2} [\tilde{\phi}(q)]^2. \end{aligned} \quad (7)$$

For the Thomas-Fermi potential Eq. 4, we have

$$\begin{aligned} \langle V^2 \rangle - \bar{V}^2 &= \frac{n_{\text{imp}}}{2\pi} \int q dq \left[ \frac{2\pi e^2}{\kappa} \frac{e^{-qd}}{q + q_{\text{TF}}} \right]^2, \\ &= 2\pi n_{\text{imp}} (e^2/\kappa)^2 C_0^{\text{TF}}(x = 2q_{\text{TF}}d), \end{aligned} \quad (8)$$

where  $C_0^{\text{TF}}(x) = \partial_x (x e^x E_1[x])$  and  $E_1[x] = \int_x^\infty dt e^{-t}/t$  is the exponential integral function. While the results presented here are for the Thomas-Fermi potential Eq. 4, it is straightforward to generalize this result to obtain  $C_0^{\text{RPA}}$  for RPA screening (e.g. using the numerical bilayer dielectric function calculated in Ref. 31), but for the relevant density scale set by  $q_{\text{TF}}$ , we expect these results to be quantitatively quite similar. The self-consistent

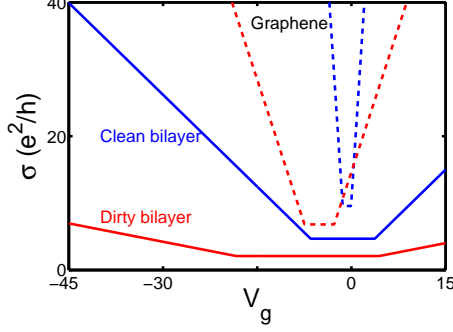


FIG. 2: (Color online) Self-consistent Boltzmann theory for bilayer graphene (solid lines) compared with results of Ref. 11 for monolayer graphene (dashed lines).

density  $n^*$  is found by setting  $E_F^2 = \langle \delta V^2 \rangle$  (see discussion in Refs. 11,12) where this approximation ignores the exchange and correlation contributions which are believed to be small.<sup>10,29,30</sup> Applying this self-consistent procedure to bilayer graphene, we find  $(\pi n^*/2m)^2 = 2\pi n_{\text{imp}}(e^2/\kappa)^2 C_0^{\text{TF}}$  and

$$\begin{aligned} n^* &= \sqrt{n_{\text{imp}} \tilde{n}}, \\ \tilde{n} &= \frac{1}{2\pi} q_{\text{TF}}^2 C_0^{\text{TF}} (2q_{\text{TF}} d) \\ &\approx 140 \times 10^{10} \text{cm}^{-2}, \end{aligned} \quad (9)$$

where we approximate  $C_0^{\text{TF}}(x \approx 1) \approx 0.085$ . This disorder induced residual density gives rise to a non-vanishing conductivity even as the external gate voltage is tuned through zero.

#### IV. SELF-CONSISTENT TRANSPORT THEORY

Combining the low and high density results developed in the preceding sections, we find for bilayer graphene

$$\sigma(n - \bar{n}) = \begin{cases} \frac{4e^2}{\pi h} \sqrt{\frac{\tilde{n}}{n_{\text{imp}}}} & \text{if } n - \bar{n} < n^*, \\ \frac{4e^2}{\pi h} \frac{n}{n_{\text{imp}}} & \text{if } n - \bar{n} > n^*, \end{cases} \quad (10)$$

where  $\bar{n} = n_{\text{imp}}$  and  $\tilde{n} \approx 140 \times 10^{10} \text{cm}^{-2}$ . This result predicts that a reasonably clean bilayer sample with  $n_{\text{imp}} = 5 \times 10^{10} \text{cm}^{-2}$  would have a mobility  $\mu \sim n_{\text{imp}}^{-1} \approx 6000 \text{cm}^2/\text{Vs}$ . The residual density  $n^* = \sqrt{n_{\text{imp}} \tilde{n}} \sim 25 \times 10^{10} \text{cm}^{-2}$  with a plateau width  $\Delta V \sim 4V$  and minimum conductivity  $\sigma_{\text{min}} \sim 7e^2/h$ . When compared to recent experimental results,<sup>34</sup> these estimates agree well for the mobility, plateau width and minimum conductivity, although not for the offset gate voltage determined from  $\bar{n}$  (see Refs. 35,36 for a discussion of other factors that could determine the threshold voltage shifts and could

account for this discrepancy). These results do not depend qualitatively on the precise choice of  $d$ , although the results do depend quantitatively; for example, for the same value of  $n_{\text{imp}}$ , increasing  $d$  by a factor of 2 gives  $n^* \approx 15 \times 10^{10} \text{cm}^{-2}$ . This may be important for bilayer graphene, since the distance between the two layers  $c \sim 0.3 \text{nm}$  suggests that for the same substrate, the effective distance from the charged impurities would be larger for bilayers than for graphene. The results of Eq. 10 are shown in Fig. 2 for both a clean ( $n_{\text{imp}} = 10^{11} \text{cm}^{-2}$ ) and dirty ( $n_{\text{imp}} = 5 \times 10^{11} \text{cm}^{-2}$ ) samples and compared with the results of Ref. 11 for graphene using the same charged impurity densities and keeping  $d = 1 \text{nm}$  fixed. One notices immediately that for the same charged impurity concentration, graphene has a factor of 16 higher mobility, smaller plateau widths and larger minimum conductivities than the bilayer system. These predictions can be easily tested in future experiments. We also note that only  $\sigma(n) \sim n$  behavior was observed in the experiments of Ref. 34 indicating that the current experiments are adequately described by the complete screening approximation, although future experiments should observe a “super-linear” conductivity (i.e.  $\alpha > 1$ ) at higher density arising both from the high-density Thomas-Fermi corrections as well as from the high-density graphene bilayer Hamiltonian crossing over from quadratic to linear.

#### V. TEMPERATURE DEPENDENCE

Shown in the Fig 1 is the effect of chirality on the dominant scattering angle, where the suppression of backscattering seen in graphene is absent for bilayer graphene. It was argued recently that the suppression of  $2k_F$  scattering in graphene implied weak temperature dependence<sup>18</sup> until higher temperatures where phonon effects are observed. The fact that  $2k_F$  scattering is not suppressed in bilayer graphene does not, however, necessarily lead to any screening (or equivalently, Friedel oscillation) induced strong temperature dependence in the resistivity. The temperature dependence in bilayer graphene depends on three dimensionless parameters:  $q_{\text{TF}}/2k_F$ ;  $T/T_F$ ; and  $T/T_D$  where  $T_D \approx \hbar/2\tau$  is the Dingle temperature and  $T_F$  is the Fermi temperature. The temperature dependence from screening will be weak if any one of these three parameters is not large.

The actual value of the dimensionless screening parameter

$$\begin{aligned} \frac{q_{\text{TF}}}{2k_F} &= \frac{2me^2}{\kappa \hbar^2 \sqrt{\pi n}}, \\ &\lesssim \frac{2me^2}{\kappa \hbar^2 \sqrt{\pi n^*}} \approx 6, \end{aligned} \quad (11)$$

is reasonably small even at the lowest accessible carrier density set by  $n^* \sim 2.5 \times 10^{11} \text{cm}^{-2}$ , making the temperature dependence arising from screening rather weak. Second, the dimensionless temperature  $T/T_F$  is rather small

since the Fermi temperature  $T_F$  changes from 120 K at low density (set by  $n^*$ ) to 1200 K at high density (set by  $n = k_F^2/\pi = aV_g \approx 3.6 \times 10^{12} \text{ cm}^{-2}$ , where  $a \approx 7.2 \times 10^{10} \text{ cm}^{-2}\text{V}$  is a geometry related factor).

The Fermi temperature is relatively high due to the very small carrier effective mass ( $\approx 0.03 m_e$ ) in bilayer graphene. In fact, the effective mass for bilayer graphene is less than half of that for 2D electrons in GaAs ( $\approx 0.07 m_e$ ), where the temperature dependence arising from screening is extremely small<sup>28</sup> even at much lower carrier densities. Therefore, we do not anticipate any strong screening-induced temperature dependence in bilayer graphene resistivity. Finally, the currently available bilayer graphene samples have very small mobilities resulting in relatively strong collisional broadening effects (i.e. high Dingle temperature) which would suppress any small screening induced temperature dependence that could have arisen at low temperatures. In particular, a mobility of  $5000 \text{ cm}^2/\text{Vs}$  as observed in Ref. 34 corresponds to a  $T_D \sim 50 \text{ K}$ , leading to further suppression of any screening induced temperature dependence in the conductivity.

It is therefore gratifying to see that the recent experiment on bilayer graphene<sup>34</sup> does not see much temperature dependence in the low temperature resistivity in spite of the importance of  $2k_F$  scattering in bilayer graphene. The temperature dependence seen in the plateau region is likely to be caused by thermal population of carriers since  $T_F \approx 120 \text{ K}$ , and the temperature dependence is seen for  $T \gtrsim 100 \text{ K}$ . For  $T \gg T_F$ , the thermally excited carrier density  $n(T) = \int \nu(\varepsilon) f(\varepsilon, T) d\varepsilon$ , where  $f(\varepsilon, T)$  is the Fermi distribution function. This gives  $n \sim T$  for bilayer graphene, while  $n \sim T^2$  for graphene giving for the conductivity (ignoring any phonon or electron-hole scattering contributions)

$$\sigma(T \gg T_F) = \begin{cases} \frac{8 \ln 2}{\pi^2 h} \frac{m e^2}{\hbar^2 n_{\text{imp}}} (kT) & \text{for bilayers,} \\ \frac{10 \pi e^2}{3 h} \frac{1}{n_{\text{imp}} \hbar^2 v_F^2} (kT)^2 & \text{for graphene.} \end{cases} \quad (12)$$

Note that the thermal excitation of carriers leads to an enhanced<sup>34</sup>  $\sigma(T)$  whereas temperature dependent  $2k_F$  screening typically suppresses  $\sigma(T)$ . For bilayer graphene, this result suggests that for  $T \approx 260 \text{ K}$ , there would be a 300 percent enhancement in the minimum conductivity which is consistent with the observations and estimates of Ref. 34. The situation for single layer graphene is quite different, since even in the low density saturation regime,  $T/T_F \ll 1$ . For example, a residual density  $n^* = 2.5 \times 10^{11} \text{ cm}^{-2}$  corresponds to  $T_F \approx 100 \text{ K}$  for bilayer graphene and  $T_F \approx 700 \text{ K}$  for single layer graphene. For this reason, one expects the minimum conductivity in bilayer graphene to show stronger temperature dependence than single layer graphene even though Eq. 12 shows the bilayer conductivity scaling as  $\sim T$  (compared to  $\sigma \sim T^2$  for the monolayer).

## VI. CONCLUSION

The formalism developed here captures many features of graphene bilayer transport. In particular, we show that both the low density saturation and the high-density linear in density behavior seen in recent experiments arise from the same charged impurities that are invariably present in samples exfoliated onto a  $\text{SiO}_2$  substrate. We note that the agreement between our self-consistent Boltzmann theory and available graphene (and bilayer) transport experiments and direct measurement of the electron and hole puddles giving rise to the residual density, indicate that in current experiments, most of the charged impurities reside close to the graphene-substrate interface (i.e. within  $\sim 1 \text{ nm}$ ) similar to the corresponding situation in Si-SiO<sub>2</sub> MOSFET structures. If the typical distance of impurities from the graphene (or bilayer) sheet could be changed in future experiments (e.g. by removing the  $\text{SiO}_2$  substrate), the formalism we have developed predicts quantitatively its effect on transport properties and on the magnitude of the electron and hole puddles. Another conclusion of our work is that bilayer mobilities are an order of magnitude smaller than corresponding mobilities for graphene samples on similar substrates. We also argue that the minimum conductivity, plateau width and threshold voltage have different scaling in graphene and bilayers and have different dependence on the substrate dielectric constant. These differences could potentially be useful when designing a particular device application. Moreover, a systematic study of the differences in transport properties between single layer graphene and bilayer graphene could verify our claim that the underlying mechanism for most of the observed transport properties on current graphene (and bilayer) samples is dominated by charged impurities.

In addition we have argued that both graphene and bilayers have weak temperature dependence making these materials have among the highest room temperature mobility for any field effect device. One important consequence for technology is that since mobility is limited by charged impurities, better samples can be made either by removing charged impurities in the  $\text{SiO}_2$  substrate or by using different substrate (e.g. vacuum for the case of suspended graphene and bilayers). Attaining high mobility is also necessary to access new physics such as the fractional quantum Hall effect or the “universal” minimum conductivity, both of which we believe is not seen in current experiments due to the large number of charged impurities.

In one sense, bilayer graphene can be thought of as a new material that shares some properties with regular 2DEGs (e.g. quadratic Hamiltonian) and some properties with graphene (e.g. chiral Hamiltonian). However, theoretically, bilayer graphene is a far more interesting, where as discussed earlier, modestly increasing the back gate voltage from that of current experiments should induce a sufficiently large carrier density to see several interesting effects. For example, a “super-linear” con-

ductivity is predicted both by high-density corrections in the Thomas-Fermi approximation (within the quadratic Hamiltonian) as well as by the theoretically expected crossover between the quadratic and linear Hamiltonians. At even higher (and perhaps realistic) densities, one would expect a strong increase conductivity as one populated higher bands. The theoretical framework for understanding these high-density effects (including the role of chirality) and their observation remains an exciting avenue for future theoretical and experimental research. In summary, we have proposed a simple theory for bi-

layer graphene transport including the effects of screened Coulomb impurities. The result of our self-consistent Drude-Boltzmann semi-classical diffusive transport theory<sup>11</sup> is in good agreement with the recent experiments of Ref. 34 and we make several predictions that can be tested in future experiments.

We thank Andre Geim for sharing with us his unpublished data (Ref. 34) and for a careful reading of our manuscript. This work is supported by U.S. ONR.

- 
- <sup>1</sup> S. Das Sarma, A. K. Geim, P. Kim, and A. H. MacDonald, eds., *Exploring Graphene: Recent Research Advances, A Special Issue of Solid State Communications*, vol. 143 (Elsevier, 2007).
  - <sup>2</sup> E. McCann and V. Fal'ko, Phys. Rev. Lett. **96**, 086805 (2006).
  - <sup>3</sup> J. Nilsson, A. Castro Neto, N. Peres, and F. Guinea, Phys. Rev. B **73**, 214418 (2006).
  - <sup>4</sup> B. Partoens and F. Peeters, Phys. Rev. B **74**, 075404 (2006).
  - <sup>5</sup> M. Koshino and T. Ando, Phys. Rev. B **73**, 245403 (2006).
  - <sup>6</sup> I. Snymen and C. Beenakker, Phys. Rev. B **75**, 045322 (2007).
  - <sup>7</sup> K. Novoselov, E. McCann, S. Morozov, V. Fal'ko, M. Katsnelson, U. Zeitler, D. Jiang, F. Schedin, and A. Geim, Nature Physics **2**, 177 (2006).
  - <sup>8</sup> J. Oostinga, H. Heersche, X. Liu, A. Morpurgo, and L. Vandersypen, Nature Materials **7**, 151 (2008).
  - <sup>9</sup> J. Nilsson and A. Castro Neto, Phys. Rev. Lett. **98**, 126801 (2007).
  - <sup>10</sup> H. Min, B. Sahu, S. K. Banerjee, and A. H. MacDonald, Phys. Rev. B **75**, 155115 (2007).
  - <sup>11</sup> S. Adam, E. H. Hwang, V. M. Galitski, and S. Das Sarma, Proc. Natl. Acad. Sci. USA **104**, 18392 (2007).
  - <sup>12</sup> B. I. Shklovskii, Phys. Rev. B **76**, 233411 (2007).
  - <sup>13</sup> Y.-W. Tan, Y. Zhang, K. Bolotin, Y. Zhao, S. Adam, E. H. Hwang, S. Das Sarma, H. L. Stormer, and P. Kim, Phys. Rev. Lett. **99**, 246803 (2007).
  - <sup>14</sup> J. H. Chen, C. Jang, S. Adam, M. S. Fuhrer, E. D. Williams, and M. Ishigami, Nature Physics, in press (arXiv:0708.2408v1) (2008).
  - <sup>15</sup> J. Martin, N. Akerman, G. Ulbricht, T. Lohmann, J. H. Smet, K. von Klitzing, and A. Yacobi, Nature Physics **4**, 144 (2008).
  - <sup>16</sup> K. Nomura and A. H. MacDonald, Phys. Rev. Lett. **98**, 076602 (2007).
  - <sup>17</sup> T. Ando, J. Phys. Soc. Jpn. **75**, 074716 (2006).
  - <sup>18</sup> V. Cheianov and V. Fal'ko, Phys. Rev. Lett. **97**, 226801 (2006).
  - <sup>19</sup> E. H. Hwang, S. Adam, and S. Das Sarma, Phys. Rev. Lett. **98**, 186806 (2007).
  - <sup>20</sup> T. Stauber, N. M. R. Peres, and F. Guinea, Phys. Rev. B **76**, 205423 (2007).
  - <sup>21</sup> K. Kechedzhi, V. Fal'ko, E. McCann, and B. Altshuler, Phys. Rev. Lett. **98**, 176806 (2007).
  - <sup>22</sup> R. V. Gorbachev, F. V. Tikhonenko, A. S. Mayorov, D. W. Horsell, and A. K. Savchenko, Phys. Rev. Lett. **98**, 176805 (2007).
  - <sup>23</sup> M. Katsnelson, Eur. Phys. J. B **52**, 151 (2006).
  - <sup>24</sup> M. Katsnelson, Phys. Rev. B **76**, 073411 (2007).
  - <sup>25</sup> J. Cserti, Phys. Rev. B **75**, 033405 (2007).
  - <sup>26</sup> T. Ando, A. B. Fowler, and F. Stern, Rev. Mod. Phys. **54**, 437 (1982).
  - <sup>27</sup> S. Adam, E. Hwang, and S. Das Sarma, Physica E **40**, 1022 (2008).
  - <sup>28</sup> M. P. Lilly, J. L. Reno, J. A. Simmons, I. B. Spielman, J. P. Eisenstein, L. N. Pfeiffer, K. W. West, E. H. Hwang, and S. Das Sarma, Phys. Rev. Lett. **90**, 056806 (2003).
  - <sup>29</sup> E. H. Hwang and S. Das Sarma, Phys. Rev. B **75**, 205418 (2007).
  - <sup>30</sup> Y. Barlas, T. Pereg-Barnea, M. Polini, R. Asgari, and A. H. MacDonald, Phys. Rev. Lett. **98**, 236601 (2007).
  - <sup>31</sup> X. Wang and T. Chakraborty, Phys. Rev. B **75**, 041404 (2007).
  - <sup>32</sup> V. Cheianov, V. Fal'ko, B. Altshuler, and I. Aleiner, Phys. Rev. Lett. **99**, 176801 (2007).
  - <sup>33</sup> V. Galitski, S. Adam, and S. Das Sarma, Phys. Rev. B **76**, 245405 (2007).
  - <sup>34</sup> S. V. Morozov, K. S. Novoselov, M. I. Katsnelson, F. Schedin, D. C. Elias, J. A. Jaszczak, and A. K. Geim, Phys. Rev. Lett. **100**, 016602 (2008).
  - <sup>35</sup> E. H. Hwang, S. Adam, and S. Das Sarma, Phys. Rev. B **76**, 195421 (2007).
  - <sup>36</sup> F. Schedin, A. K. Geim, S. V. Morozov, D. Jiang, E. H. Hill, P. Blake, and K. S. Novoselov, Nature Materials **6**, 652 (2007).